Ru-Pyrochlores: Compositional Tuning for Electrochemical Stability as Cathode Materials for IT-SOFCs

G. Ehora,[†] S. Daviero-Minaud,*[,†] M. C. Steil,[‡] L. Gengembre,[†] M. Frère,[†] S. Bellayer,[§] and O. Mentré[†]

Unité de Catalyse et de Chimie du Solide (UCCS), UMR CNRS 8181 ENSCL, Bât. C7 BP 90108, 59652 Villeneuve d'Ascq Cedex, France, Laboratoire d'Electrochimie et de Physicochimie des Matériaux et des Interfaces (LEPMI), ENSEEG-INP Grenoble, BP 75, 38402 Saint Martin d'Hères Cedex, France, and Laboratoire des Procédés d'Élaboration des Revêtements Fonctionnels (PERF), LSPESUMR-CNRS 8008, ENSCL, Bât. C7 BP 90108, 59652 Villeneuve d'Ascq Cedex, France

Received July 16, 2008. Revised Manuscript Received October 13, 2008

Using XRD, impedance spectroscopy, and XPS, it was shown that both $Bi_2Ru_2O_7$ and $Pb_2Ru_2O_{6.5}$, generally announced as attractive electrode materials for IT-SOFCs, chemically react with CGO. In addition, a never-mentioned time-instability under electrochemical measurements with YZS as electrolyte mediates the polarization tests. For $Pb_2Ru_2O_{6.5}$, long time experiments (stabilization time > 900 h, previously to complementary electrochemical tests), yields strong increasing of the resistance polarization. Concerning $Bi_2Ru_2O_7$, a partial transformation into $Bi_3Ru_3O_{11}$ is observed after impedance measurements. The investigation of the $Bi_{2-x}M_xRu_2O_{7-\delta}$ (M = Sr, Pb) solid solutions was performed with the aim to improve the catalytic/electric properties. For low x values, it shows a time and chemical stabilization of the electrode/electrolyte cells, able to preserve high electrode performances of these materials. For higher substitution, the chemical/electrochemical instability reappears. According to our polarization measurements versus oxygen pressure and temperature in the so-called "stabilized" samples, the electrode performance appears limited by the diffusion of adsorbed oxygen on the triple point boundary. It is fully compatible with the metallic behavior checked in all the series.

1. Introduction

Fuel cells are considered as one of the most promising energy generators of tomorrow; however, their developments remain limited because of the technological problems encountered for their implementation. Among the various technical solutions developed, oxides solid fuel cells (SOFCs) are promising mainly on account of their broad applications spectrum (domestic, transport, etc.) and very low pollutant emission. However, so far, their working conditions are limited to high temperatures (800−1000 °C), mainly due to the intrinsic properties of the selected solid electrolytes, for example, yttrium stabilized zirconia (YSZ). For their implementation, temperature-stable electrode materials on heating−cooling cycles, assorted with suitable electrode/electrolyte contacts, are required from the chemical and mechanical point of view. Of course, the resulting feasibility of such systems is a key limitation of today's applicability. For those reasons, the currently research and developments are directed toward SOFCs running at lower temperatures than 700 °C (intermediate temperature IT-SOFC and low temperature LT-SOFC) including the optimization of the thermodynamic and kinetic aspects involved in the electrochemical process. The required properties for cathodes involve a high electronic conductivity with possible O^{2-} contribution, a good catalytic activity toward oxygen dissociation, and a chemical and thermal stability in the concerned thermal range, as well as a good [1−4] stability toward the electrolyte.

As a result of their well-known catalytic activities toward oxygen reduction assorted to their metallic/semiconducting transport accompanied with possible oxygen vacancies, Ru-based pyrochlores appear as promising compounds for cathode materials at reasonably low temperature. In fact, their good electrochemical performances were evidenced at temperature as low as 350 °C,[1,2] particularly interesting for the future IT/LT SOFC. However, it is clear that their high cost is a major obstacle for commercial development, and a more plausible application could be the coating of metallic interconnects in these electrochemical systems.[5] Nevertheless, their exhaustive characterizations must pass through the measurement of their electrochemical performances and should now focus on their often neglected time-stability in laboratory tests. $A_2Ru_2O_{7-\delta}$ phases, also denoted as $A_2Ru_2O_6O'_{1-\delta}$ (A = Bi, Pb), have already been studied with various electrolytes: 8% yttrium stabilized zirconia (8YSZ),[6−8] ceria doped gadolinium (CGO)[9−11] or bismuth based oxides

* Corresponding author. E-mail: sylvie.daviero@ensc-lille.fr.
[†] UMR CNRS 8181 ENSCL.
[‡] ENSEEG-INP Grenoble.
[§] LSPESUMR-CNRS 8008.

(1) Horowitz, H. S.; Longo, J. M.; Horowitz, H. H. *J. Electrochem. Soc.* **1983**, *130* (9), 1851.
(2) Goodenough, J. B.; Manoharan, R.; Paranthaman, P. *J. Am. Chem. Soc.* **1990**, *112*, 2076.
(3) Prakash, J.; Tryk, D.; Yeager, E. B. *J. Electrochem. Soc.* **1999**, *146*, 4145.
(4) Shulkla, A. K.; Kannan, A. M.; Hegde, M. S.; Gopalakrishnan, J. *J. Power Sources.* **1991**, *35*, 163.
(5) Zhong, Z. *Electrochem. Solid-State Lett.* **2006**, *9* (4), A215.
(6) Linquette-Mailley, S.; Caneiro, A.; Djurado, E.; Mairesse, G.; Fouletier, J. *Solid State Ionics* **1998**, *107*, 191.

10.1021/cm801942c CCC: $40.75
Published on Web 11/17/2008

(BiMEVOX or ESB).[12,13] Adapted to these latter electrolytes, the domination of the interfacial electrode/electrolyte formed phases on the cell polarization process has been evidenced,[12] but no particular time effect has been reported.

The ruthenium pyrochlore catalytic properties are related to their easy reversible redox processes based on $Ru^{4+}-Ru^{5+}$ equilibrium.[2,3,14] Moreover oxygen vacancies on the O′ site highlighted in these materials[7,15,16] are likely to favor O^{2-} motion.

Hence, we investigated the $Bi_{2-x}M_xRu_2O_{7-\delta}$ (M = Pb, Sr) solid solutions, to tune catalytic and electric properties, while exploiting the variable oxygen vacancies concentration and the mean Ru valence. Lead and strontium have been selected for the preservation of the metallic behavior in our materials. In addition, to our knowledge, the $Bi_{2-x}Sr_xRu_2O_{7-\delta}$ solid solution has never been mentioned previously and is fully characterized in the present work. An important aspect of our work also deals with the time durability of the mounted cells. In fact our work shows that this too-often neglected aspect appears as a limiting factor while the compositional tuning enables a stabilization of the electrochemical performances.

Since our work is devoted to a comparison with previous results, the standard YSZ was selected but adapted to the IT range (500−700 °C). As reported later, the pyrochlore phases and the cubic zirconia exhibit similar unit-cell parameters, leading to an excellent coherence between most of the crystallographic plans. Here, we benefited of this specificity for a good electrode/electrolyte adhesion. All the results have been analyzed by comparison with the parent Bi and Pb ruthenates.

2. Experimental Section

Powder Synthesis and Characterization. $Bi_{2-x}Pb_xRu_2O_{7-\delta}$ and $Bi_{2-x}Sr_xRu_2O_{7-\delta}$ were synthesized by solid state reaction between Bi_2O_3 (Aldrich, 99.9%), PbO (Riedel de Haën, 99%) or SrO_2 (Aldrich), and RuO_2 (Alfa Aeser, 99.9%) mixed in stoichiometric ratio, ground in an agate mortar and heated at 1000 °C during 48 h for $Bi_2Ru_2O_7$ and 72 h for the others compounds. Several intermediate grindings are necessary to obtain single phased samples. Powder X-ray diffraction (XRD) patterns have been collected using a HUBER Guinier G670 diffractometer (Cu Kα1 radiation) with an Image Plate detector, and neutron diffraction (ND) data were collected on the 3T2 diffractometer ($\lambda = 1.226286$ Å) at the LLB (Grenoble, France).

Physical Property Measurements. The magnetic susceptibility ($H = 1$ T) was measured by the DC extraction method, using an OXFORD Maglab EXA 9T magnetometer. Four-probes measurements were performed between 5 and 300 K (Maglab) and 300 and 1000 K (homemade system) on rectangular bars, uniaxially pressed and sintered at 900 °C for 10 h with a heating and cooling rate of 1.5 °C/min and 2.15 °C/min, respectively. The resistivity ρ was estimated from the resistance as $\rho = (2\pi s/F_{(a,h,l)})*R$, where s is the electrode spacing (0.34 cm) and a, h, and l are the bar dimensions that allow the determination of the correcting $F(a,h,l)$ factor.[17]

Cell Manufacturing. Symmetric cells have been prepared, all in the same conditions, for each tested pyrochlore composition. The YSZ electrolytic membrane (10 mm in diameter, 2.3 mm in thickness) was prepared by isostatic pressing of 8YSZ powder (Tosoh) and sintered at 1400 °C for 2 h. For the electrode deposition, slurries were prepared and deposited on each side of the YSZ pellets by screen painting: First, the grain size of ruthenate pyrochlores powders was reduced by ball-milling in ethanol and then mixed with a dispersant (alkyl ether phosphate acid) and an organic binder (terpenoids oils) in water. After deposition the cells were sintered at 850 °C for 2 h. Because of the possibility of compositional evolution during the thermal treatment, the electrode composition was checked by electron probe Castaing microanalyser (EPMA) after sintering. The samples were characterized using XRD, scanning electron microscopy (SEM JEOL JSM 5300), and X-ray photoelectron spectroscopy (XPS) before and after the impedance spectroscopy measurements.

Compositional Analysis. A Cameca SX100 electron probe microanalyser (EPMA) was used to perform elemental analysis. Quantifications of Sr, Bi, Ru, and Pb were carried out at 10 kV and 40 nA with a spot size of 20 μm. A TAP crystal was used to detect the Sr Lα X-rays and a PET crystal to detect the Pb and Bi Mα and the Ru Lα X-rays. Oxygen was calculated by difference to 100 wt % and taken into account for matrix corrections. Standards used for quantification were made of pure PbO, $SrCO_3$, RuO_2,and Bi_2O_3 powder pressed into small plates. Means and standard deviations were calculated from measurements carried out at five different places on each sample.

Surface Analysis. XPS analyses were performed using the ESCALAB 220XL spectrometer. The Al kα monochromatic line (1486.6 eV) was used for excitation with a 200 W applied power giving an 800 μm spot diameter on the sample. The spectrometer was operated in a constant pass energy mode (Epass = 40 eV) for high-resolution spectra recording using the electromagnetic lens mode. During the experiment the vacuum level was less than 10^{-7} Pa. Experimental quantification was obtained using the Eclipse software provided by VG Scientific. The in-depth stoichiometry variations were determined by argon etching at 3 keV and 0.8 $\mu A \cdot cm^{-2}$.

Impedance Spectroscopy. Impedance spectroscopy was carried out on a solartron 1280B in the range 10^{-3} to 2×10^4 Hz. The signal amplitude imposed during measurements is low enough (30−50 mV) for a 0-current approximation. The impedance spectra are treated and refined using ZView 2.9c.[18] Spectra were recorded in the temperature range 430−650 °C. Below 430 °C, it becomes necessary to impose higher signal amplitude (>50 mV) to obtain exploitable impedance diagrams. The possible induced cell polarization is such that only the $Bi_{1.5}Sr_{0.5}Ru_2O_{7-\delta}$/YSZ/$Bi_{1.5}Sr_{0.5}Ru_2O_{7-\delta}$ cell was studied at lower temperatures (430−350 °C) with an amplitude signal of 100 mV. Experiments were carried out under

(7) Linquette-Mailley, S.; Djurado, E.; Mairesse, G.; Fouletier, J. *Sens. Actuators, B* **1995**, *26−27*, 364.
(8) Takeda, T.; Kanno, R.; Kawamoto, Y.; Takeda, Y.; Yamamoto, O. *J. Electrochem. Soc.* **2000**, *147* (5), 1730.
(9) Doshi, R.; Richards, V. L.; Carter, J. D.; Wang, X.; Krumpelt, M. *J. Electrochem. Soc.* **1999**, *146* (4), 1273.
(10) Jaiswal, A.; Wachsman, E. D. *J. Electrochem. Soc.* **2005**, *152* (4), A787.
(11) Bae, J.-M.; Steele, B. C. H. *J. Electroceram.* **1999**, *3* (1), 37.
(12) Esposito, V.; Traversa, E.; Wachsman, E. D. *J. Electrochem. Soc.* **2005**, *152* (12), A2300.
(13) Esposito, V.; Luong, B. H.; Di Bartolomeo, E.; Wachsman, E. D.; Traversa, E. *J. Electrochem. Soc.* **2006**, *153* (12), A2232.
(14) Zen, J. M.; Manoharan, R.; Goodenough, J. B. *J. Appl. Electrochem.* **1992**, *22* (2), 140.
(15) Kennedy, B. J. *J. Solid State Chem.* **1996**, *123*, 14.
(16) Avdeev, M.; Haas, M. K.; Jorgensen, J. D.; Cava, R. J. *J. Solid State Chem.* **2002**, *169*, 24.
(17) Laplume, J. *L'onde Electrique* **1955**, *335*, 113.
(18) *ZView 2.9c* commercial software Solartron Instrument, UK.

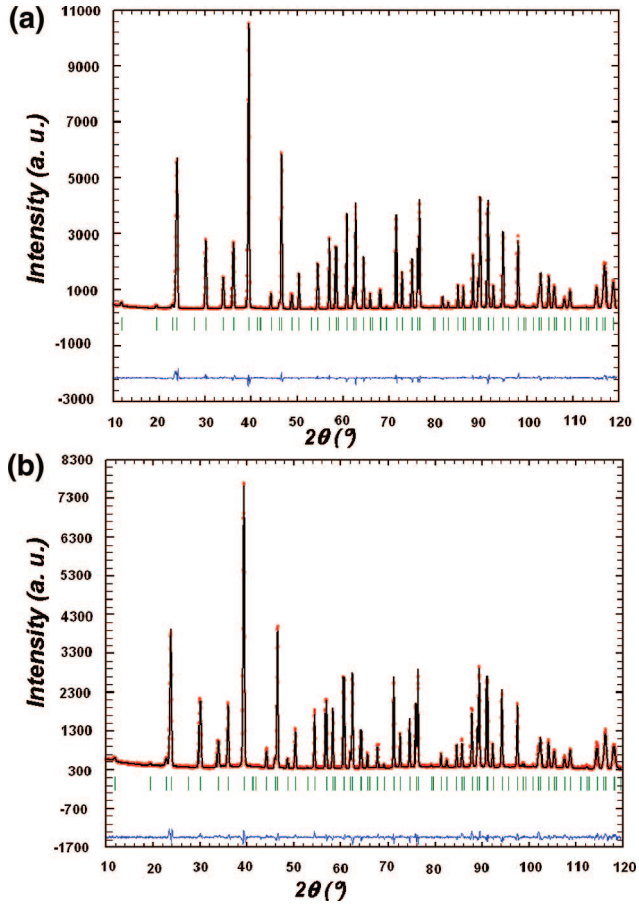

Figure 1. Rietveld ND patterns for (a) $BiPbRu_2O_{6.73}$ and (b) $Bi_{1.75}Sr_{0.25}Ru_2O_{6.9}$.

oxygen partial pressures ranging from pure oxygen (1 atm) to 10^{-6} atm using O_2/N_2gas mixtures.

3. Structural and Physical Study

3.1. Structural Characterization of the Pyrochlore Ruthenate Powders. After checking the purity, the lattice parameters of the bulk powders and positional parameters have been refined by the Rietveld method, carried out using Fullproff.[19] For $Bi_{1.75}Sr_{0.25}Ru_2O_{6.9}$ and $BiPbRu_2O_{6.73}$, ND analyses have been yielding reliable information on the δ value (Figure 1). In any case, a standard pseudo-Voigt function was used for the profile fitting. We have explored the complete $Bi_{2-x}Pb_xRu_2O_{7-\delta}$ solid-solution domain. For $Bi_{2-x}Sr_xRu_2O_{7-\delta}$, in our conditions of preparation, the solid solution exists until $x = 0.8$, after which $SrRuO_3$ impurity is detected in the samples. The refinement and structural data are gathered in the Table 1. The lattice parameters for $Bi_2Ru_2O_7$ are in good agreement with those of the literature.[20]

The ideal $Fd\bar{3}m$ space group was selected for all the refined compounds involving a statistical $\square/O^{2-}$ disorder on the 8(b) crystallographic site of O′, as commonly reported for $\delta \ll 0.5$.[21,22] Hence, in particular cases of $\square/O^{2-}$ ordered arrangement, the space group decreases to $F\bar{4}3m$ due to the ordering of O′ oxygen and vacancies into filled 4(d) and empty 4(b) positions. This particular symmetry has been observed in $Pb_2Ru_2O_{6.5}$ by the existence of additional $hk0$ ($h + k \neq 4n$) on ND patterns.[23,24] These satellites are not observable on XRD patterns and were not observed on the two available ND patterns (Figure 1), justifying the choice of the most symmetrical $Fd\bar{3}m$. It is worth recalling that the space group choice should not affect the quality of the refinement since the $A_2Ru_2O_6$ sublattice can be identically described in both space groups.

In $Bi_{2-x}Pb_xRu_2O_{7-\delta}$, the plot of the lattice parameter versus x (Figure 2) is concave upward with a maximum around $x = 0.5$. It is related to the interaction of two opposite effects: (i) the Bi^{3+} (ionic radius = 0.96 Å) substitution for slightly larger Pb^{2+} (ionic radius = 0.98 Å)[25] and (ii) the creation of vacancies with increasing x. Of course, the former effect largely predominates in the case of the substitution for large Sr^{2+} (i.r. = 1.18 Å) in the narrow solid solution range. The most relevant distances A−O and Ru−O for all compounds are given Table 1. Generally, the introduction of larger species (Pb^{2+}, Sr^{2+}) is followed by an enlargement of the size of the hexagonal tunnels; that is, A−O′ and A−O increase, while the RuO_6 based framework is subsequently compressed, that is, decrease of Ru−O bond lengths.

3.2. Magnetic and Electric Properties. The metallic conducting properties of $Bi_2Ru_2O_7$ and $Pb_2Ru_2O_{6.5}$ arise from the interactions between RuO_6 octahedra and Bi,Pb−O′ via the Ru−O−(Bi, Pb) connections.[26,27] Indeed, it has been shown that unoccupied 6p states of bismuth or lead, near the Fermi level E_F, contribute to metallic conductivity by the mixing of 4d state of the Ru via the oxygen framework. Then geometrical considerations showed the importance of the effects of the O−Ru−O bonds angles and Ru−O distances on the electrical properties, for different doping elements, modifying the overlapping.[28−31] Several parameters are reported to play in favor of the metallic properties: (i) the occupancy of the A site of a polarizable cation (Bi^{3+}, Pb^{2+}, Tl^{+}...); (ii) the Ru−O−Ru angles greater than 133°; (iii) Ru−O distances shorter than 2 Å; and (iv) the presence of oxygen vacancies reminiscent of lattice contraction and mixed valence state. Because most of these features are gathered in all the concerned compounds (Table 1), it is not surprising that we observed a metallic conducting behavior associated with Pauli paramagnetism (see Supporting Information, Figure a,b). Here, the values of the Ru−O−Ru angles should be considered with precaution for XRD data refinements considering the refinable x coordinate for the O

(19) FULLPROF software: Rodriguez-Carvajal, J. *Physica B*, **1993**, *192*, 55.
(20) Facer, G.; Elcombe, M. M.; Kennedy, B. J. *Aust. J. Chem.* **1993**, *46*, 1897.
(21) Kennedy, B. J. *J. Solid State Chem.* **1995**, *119*, 254.
(22) Ismunandar; Kennedy, B. J.; Hunter, B. A. *Mater. Res. Bull.* **1999**, *34*, 1263.
(23) Beyerlein, R. A.; Horowitz, H. S.; Longo, J. M.; Leonowitz, M. E.; Jorgensen, J. A.; Rotella, F. *J. Solid State Chem.* **1984**, *51*, 253.
(24) Kennedy, B. J.; Vogt, T. *J. Solid State Chem.* **1996**, *126*, 261.
(25) Shannon, R. D. *Acta Crystallogr.* **1976**, *A32*, 751.
(26) Kennedy, B. J.; Vogt, T. *J. Solid State Chem.* **1996**, *126*, 261.
(27) Lee, K. S.; Seo, D. K.; Whangbo, M. H. *J. Solid State Chem.* **1997**, *131*, 405.
(28) Cox, P. A.; Goodenough, J. B.; Tavener, J. P.; Telles, D.; Egdell, R. G. *J. Solid State Chem.* **1986**, *62*, 360.
(29) Koo, H.; Whangbo, M. H.; Kennedy, B. J. *J. Solid State Chem.* **1998**, *136*, 269.
(30) Field, M.; Kennedy, B. J.; Hunter, B. A. *J. Solid State Chem.* **2000**, *151*, 25.
(31) Li, L.; Kennedy, B. J. *Chem. Mater.* **2003**, *15*, 4060.

Table 1. Refinement Results and Structural Data with Ru−O−Ru Bond Angles and Ru−O Distance Evolutions of $Bi_{2-x}Sr_xRu_2O_{7-\delta}$ and $Bi_{2-x}Pb_xRu_2O_{7-\delta}$ Solid Solutions

	$x = 0$	$x_{Sr} = 0.1$	$x_{Sr} = 0.25^a$	$x_{Sr} = 0.5$	$x_{Sr} = 0.8$	$x_{Pb} = 0.5$	$x_{Pb} = 1^a$	$x_{Pb} = 1.5$	$x_{Pb} = 2$
a (Å)									
(RX)	10.28306(5)	10.29299(4)		10.3234(2)	10.3299(4)	10.2932(2)		10.2755(2)	10.2621(3)
(DN)	10.295[b]		10.3109(1)				10.27773(1)		10.2758[b]
δ	0.1		0.11(1)				0.27(1)		0.5
d(Ru−O) (RX)	1.939(1)	1.943(1)		1.976(1)	1.963(1)	1.961(1)		1.950(1)	1.972(1)
									1.9546(1)
(DN)	1.984[b]		1.982(1)				1.972(1))		1.969[b]
									1.954[b]
Ru−O−Ru									
(RX)	139.207(6)	138.911(5)		134.852(4)	136.991(4)	136.247(5)		137.362(5)	139.489(8)
(DN)	133.14[b]		133.779(4)				134.196(4)		134.88[b]
χ^2	0.94	1.76	1.03	0.35	0.34	0.3	1.08	0.407	0.566
R_{Bragg} (%)	4.56	3.58	2.94	3.20	6.52	4.62	3.43	3.91	4.96
Rf (%)	3.51	3.04	2.13	4.99	13.8	9.16	2.37	3.82	6.40
Rp (%)	17	12.9	9.04	21.2	54.2	21.0	6.79	16.0	18.0
Rwp (%)	13.6	11.5	8.52	10.2	15.1	11.2	7.05	9.4	9.7
Rexp (%)	15.12	9.07	8.47	29.95	42.54	23.4	6.82	23.13	26.66

[a] From this study. [b] Bibliographic ref 21.

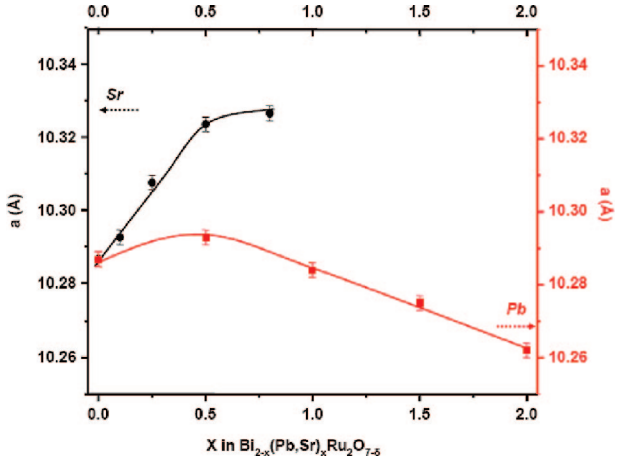

Figure 2. Lattice parameters versus x for $Bi_{2-x}(Sr,Pb)_xRu_2O_{7-\delta}$.

site of the $M_2Ru_2O_6$ sublattice. At least, our neutrons diffraction data for $x_{Sr} = 0.25$ and $x_{Pb} = 1$ fit their values greater than 133°.

As a matter of fact, the AC magnetic molar susceptibility χ_m shows almost the same evolution for all substituted compounds (Supporting Information, Figure a): Up to 50 K, χ is very low (around 7×10^{-3} emu/mol) and nearly temperature independent. At lower temperature, a Curie−Weiss contribution is observed which is reminiscent of intrinsic paramagnetic impurities (grain boundaries, defects, etc.) and of a possible second phase not detected by XRD. This Pauli-type paramagnetism has already been described by Tachibana et al.[32] and Longo et al.[33] for $Bi_2Ru_2O_7$ and $Pb_2Ru_2O_{6.5}$. In contrast, Takeda et al.[8] suggested that the electrical conductivity of $Pb_2Ru_2O_{6.5}$ is higher than the one of $Bi_2Ru_2O_7$. However, in our study all the tested compounds present a metallic low resistivity values, ($<10^{-2}$ Ω cm) and can be considered as potentially good materials for SOFCs cathode, (Supporting Information, Figure b).

4. Electrochemical Study

4.1. Reactivity Tests. In order to determine the stability between the electrodes and electrolytes, reactivity tests were performed on a mixture of the ruthenates with YSZ or with CGO, sintered at 850 °C for 3 weeks or 700 °C for 1 week, respectively, and characterized by XRD.

The reactivity of the ruthenium pyrochlores with CGO is controversial. After a thermal treatment at 800−900 °C for 24 h, Bae et al.[11] have observed new extra peaks between $Bi_2Ru_2O_7$, $Pb_2Ru_2O_{6.5}$, and CGO reminiscent of solid state reaction. In contrast, Jaiswal et al.[10] announced a neutral behavior between them. This contradiction led us to recheck this particular feature. After one week at 700 °C, the XRD patterns of the ruthenate pyrochlores powders mixed with CGO revealed their degradation into RuO_2. For this reason no further investigations have been carried on with this electrolyte. The XRD pattern of mixed $Bi_2Ru_2O_7$/CGO is given in Figure 3a.

Figure 3b shows an example of the XRD patterns after the reactivity test, carried out during three weeks at 850 °C, of the pyrochlore compounds and 8YSZ mixture. No extra peaks were evidenced, but some very small peaks attributed to monoclinic ZrO_2 are observed in the case of $Bi_2Ru_2O_7$. Takeda et al.[8] explained this phenomenon by the reaction of 8YSZ with the sillenite phase $Bi_{12}RuO_{20}$ which can be present as impurity but not detected by XRD. Then, $Bi_2Ru_2O_7$ powder has to be carefully rinsed with diluted nitric acid. 8YSZ was selected as the most convenient electrolyte in our study.

4.2. Electrodes Manufacturing. In order to optimize the microstructure of the electrode, we have followed the grain size evolution versus the grinding time. The powders were mixed with acetone and ground by ball-milling (zirconate mortar with 7 t/min speed) during variable periods. The grains size was determined by SEM micrographs. Figure 4a,b,c shows the grains before ball milling and after 4 and 8 h of grinding. No significant decrease of the grains size (~2 μm) is observed after 4 h. Furthermore, longer milling time (up to 24 h) leads to the partial reduction of the pyrochlores phases with formation of ruthenium metal. Thus, all the powders were grinded for 4 h before the deposition

(32) Tachibana, M.; Kohama, Y.; Shimoyama, T.; Harada, A.; Taniyama, T.; Itoh, M.; Kawaji, H.; Atake, T. *Phys. Rev. B* **2006**, *73*, 193107.
(33) Longo, J. M.; Raccah, P. M.; Goodenough, J. B. *Mater. Res. Bull.* **1969**, *4*, 191.

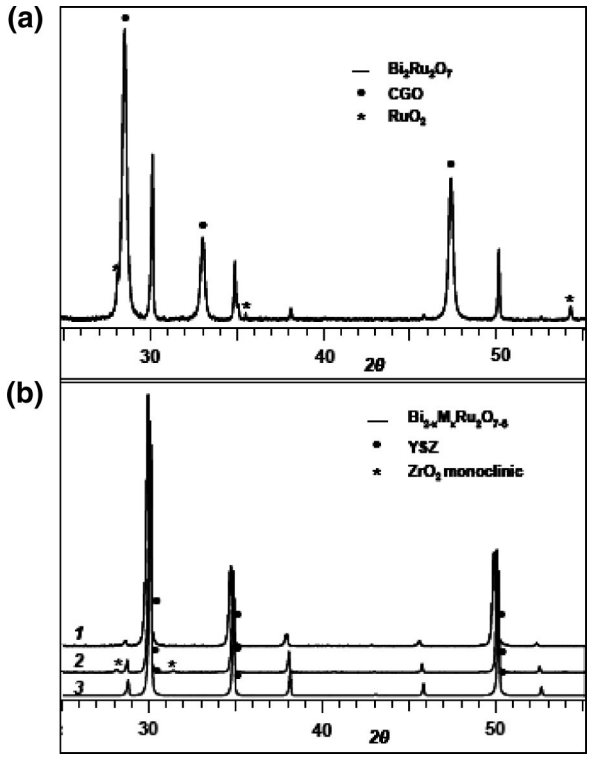

Figure 3. (a) XRD pattern of $Bi_2Ru_2O_7$−CGO mixture after 700 °C treatment for 1 week with RuO_2 extra peaks (*). (b) XRD pattern of $Bi_2Ru_2O_7Bi_{2-x}(Sr,Pb)_xRu_2O_{7-\delta}$−8YSZ mixture after 850 °C treatment for 3 weeks: weak ZrO_2 lines (*) appear after heat treatment on $Bi_2Ru_2O_7$ diffractogram.

stage (see Experimental Section). Figure 4d,e,f shows micrographs of the surface and the section of the pyrochlore electrodes on 8YSZ electrolyte pellets, after sintering at 850 °C during 2 h. The layered electrodes are homogeneous with a thickness of about 35 μm and a surface of $\sim$ 0.7 cm^2. The good adhesion between the electrode layers and the electrolyte is perceptible through the absence of cracks on the surface (Figure 4d). As expected, the very close lattice parameters of the electrolyte 8YSZ and the pyrochlore electrodes play in favor of an efficient interfacial adherence. The granular aspect of the surface with no modification of the grain size after sintering suggests a good porosity. Indeed, the micrograph of the cell section (Figure 4e,f) shows a homogeneous grain aggregation. The XRD analysis of the deposited electrode layer shows no degradation of the phases after the sintering stage, and the elemental analysis performed by EPMA gives an experimental formula closed to the nominal one (Table 2). Here, it is worth recalling that Adveev et al.[34] has shown by neutron diffraction the possibility to stabilize cation deficient Bi-based Ru pyrochlores. Our analyses show the very low deviation from the "*as prepared*" stoichiometries, even after the deposition/sintering stage.

4.3. Preliminary Polarization Tests and Time Stability. The impedance spectroscopy was carried out on several solid-solutions compositions (x = 0.1, 0.25, and 0.5 for $Bi_{2-x}Sr_xRu_2O_{7-\delta}$ and x = 0.5 and 1 for $Bi_{2-x}Pb_xRu_2O_{7-\delta}$) and on $Bi_2Ru_2O_7$ and $Pb_2Ru_2O_{6.5}$ as references. Due to the metallic comportment of the selected materials, the electrochemical performances of the electrodes are mainly related to the electrochemical mechanism occurring at the triple phase boundary (TPB), that is, O_2 gas diffusion/dissociative adsorption of O_2 molecules/diffusion of O^{2-} toward the cathode−electrolyte interface.[10,35−37] Here, the TPB is defined as the contact between the gaseous phase, the electrode, and the electrolyte. It is noteworthy that even if neglectable in term of total conductivity, a partial O^{2-}/e^- semipermeability arising from oxygen vacancies could enhance the electrode performances.

The intercept value of the impedance arcs with the real axis at the high frequency side of the Nyquist diagram corresponds to the resistance of the electrolyte and wires, while the intercept value at low frequency is attributed to the total polarization resistance (Rp). The area specific resistance (ASR) values are obtained after normalization of the Rp by the electrode surface, according to the formula ASR = (Rp × S)/2 where S is the surface of the deposited electrode in cm^2. The half-normalization assumes an averaging of the polarization at both sides of the cell.

As far as we know, the concerned literature does not mention any problem of time stability for deposited Ruthenate electrodes. In that sense, the observation in our study of pronounced time-dependent behaviors should be considered as a warning for possible unexpected phenomena. Here, we defined our own stability criteria based on three successive measurements at 650 °C ($\Delta t \approx$ 24 h) of Rp that should not evolve of more than 10%. Figure 5 shows an example of impedance spectra at 650 °C under air for $Bi_{1.9}Sr_{0.1}Ru_2O_{7-\delta}$ and $Pb_2Ru_2O_{6.5}$. In the former, Rp is stabilized after 400 h, in contrast to $Pb_2Ru_2O_{6.5}$ which still evolves after 900 h. Table 3 reports the initial and final ASR values for all tested compositions accompanied by the mention of their stability or not. In the case of $Pb_2Ru_2O_{6.5}$, a sensitive evolution of the ASR from 490 to 1090 $\Omega\cdot cm^2$ is observed. The same behavior is observed for number of the compounds considered "unstable". On the opposite, for low x values (x = 0.1−0.25 for M = Sr and until x = 0.5 for M = Pb) the $Bi_{2-x}M_xRu_2O_{7-\delta}$ solid solutions show relatively low ASR values, close to the $Bi_2Ru_2O_7$ one ($\sim$13 $\Omega\cdot cm^2$), and are considered "stable".

To our knowledge, such behavior has not been previously mentioned for ruthenium pyrochlore as electrodes adapted to YSZ. On the contrary, in their study Takeda et al.[8] have presented a lower DC resistivity for the lead ruthenate than for the bismuth ruthenate and also a lower cathodic overpotentials on 8YSZ, indicating that $Pb_2Ru_2O_{6.5}$ could be a better electrode material than $Bi_2Ru_2O_7$. Moreover, the study of $Pb_2Ru_2O_{6.5}$ on $(Er_2O_3)_{0.2}(Bi_2O_3)_{0.8}$ (ESB) carried out by Esposito et al.[12] has also shown interesting performances. According to our results, in addition to its electrochemical instability, it exhibits the worst performances. About that

(34) Avdeev, M.; Haas, M. K.; Jorgensen, J. D.; Cava, R. J. *J. Solid State Chem.* **2002**, *169*, 24.
(35) Jorgensen, M. J.; Mogensen, M. *J. Electrochem. Soc.* **2001**, *148* (5),), A433.
(36) Mogensen, M.; Primdhal, S.; Jorgensen, M. J.; Bagger, C. *J. Electroceram.* **2000**, *5* (2), 141.
(37) Adler, S. B. *Chem. Rev.* **2004**, *104*, 4791.

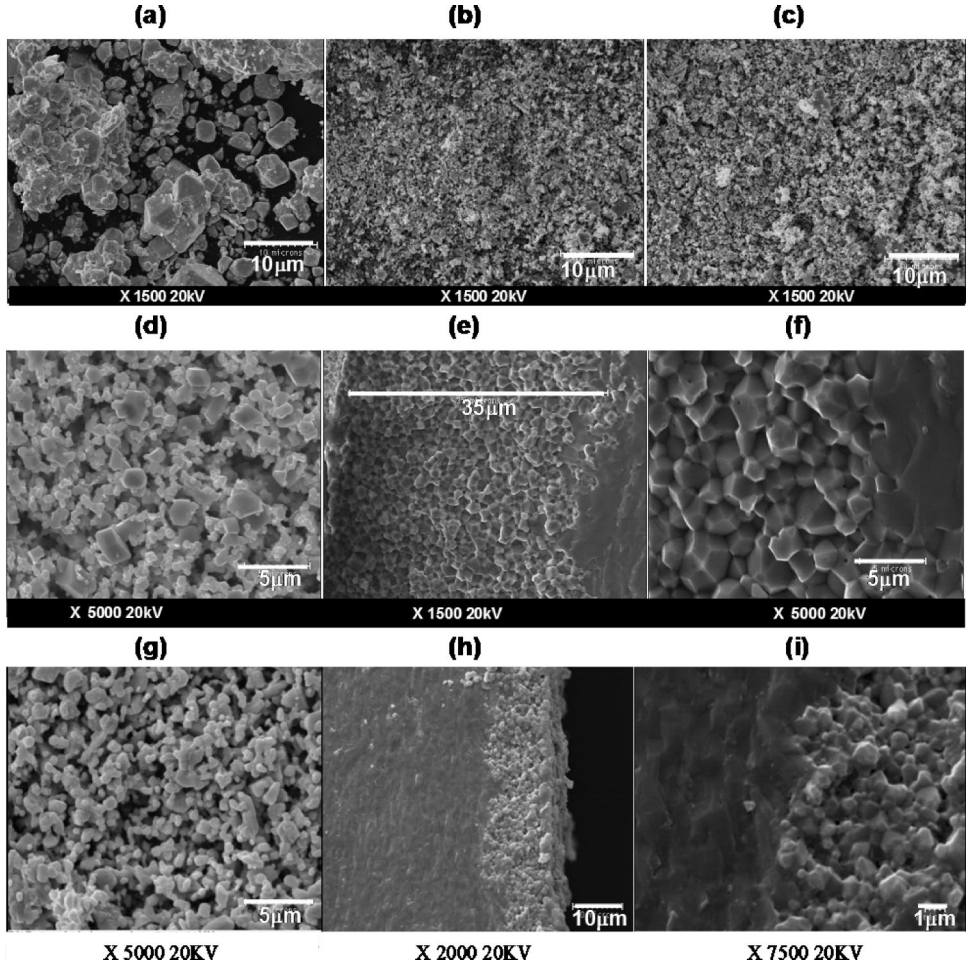

Figure 4. SEM of $BiPbRu_2O_{7-\delta}$ powder (a) as-prepared and after 4 h (b) and 8 h (c) ball-milling: the grains size remains between (b) and (c). Micrographs of the $BiPbRu_2O_7$ electrode surface (d) and section (e, f) with a zoom of the interface with 8YSZ (f). After impedance measurements: surface (g) and microsectional (h and i) micrographs of $Bi_2Ru_2O_{7-\delta}$ electrode deposited on 8YSZ.

Table 2. EPMA Analysis of the Cathode Composition and XPS Analysis Results before and after the Impedance Measurements[a]

nominal formulation	EPMA analysis atom % ± δ				EPMA formulation	XPS before impedance	XPS after impedance	XPS after scraping	unchanged RX pattern after impedance
$Bi_2Ru_2O_{7-\delta}$	Bi	Ru	O		$Bi_{2.1(1)}Ru_{2.0(3)}O_{6.9(4)}$				yes
	18.2	19.6	62.1						
	1.0	2.3	4.0						
$Bi_{1.9}Sr_{0.1}Ru_2O_{7-\delta}$	Bi	Sr	Ru	O					yes
	16.5	1.2	18.2	65.0	$Bi_{1.81(4)}Sr_{0.13(5)}$				
	0.3	0.4	0.5	1.0	$Ru_{2.00(6)}O_{7.1(1)}$				
$Bi_{1.75}Sr_{0.25}Ru_2O_{6.9}$	Bi	Sr	Ru	O					yes
	15.6	3.0	18.0	63.3	$Bi_{1.71\ (9)}Sr_{0.33\ (4)}$	$Bi_{1.70}Sr_{0.3}$	$Bi_{1.73}Sr_{0.26}$	(5 min) $Bi_{1.68}Sr_{0.32}Ru_{1.24}O_x$; (30 min) $Bi_{1.6}Sr_{0.4}Ru_{2.02}O_x$	
	0.8	0.3	0.8	1.9	$Ru_{1.98\ (9)}O_{6.9(2)}$	$Ru_{0.59}O_{4.54}$	$Ru_{0.58}O_{4.32}$		
$Bi_{1.5}Sr_{0.5}Ru_2O_{7-\delta}$	Bi	Sr	Ru	O					no
	14.1	4.0	18.7	63.1	$Bi_{1.55(9)}Sr_{0.44(5)}$	$Bi_{1.75}Sr_{0.25}$	$Bi_{1.53}Sr_{0.46}$		
	0.8	0.4	1.0	2.1	$Ru_{2.05(5)}O_{6.9(2)}$	$Ru_{0.37}O_{4.84}$	$Ru_{0.59}O_{4.87}$		
$Bi_{1.5}Pb_{0.5}Ru_2O_{7-\delta}$	Bi	Pb	Ru	O					yes
	14.1	4.0	18.7	63.1	$Bi_{1.39(4)}Pb_{0.48(3)}$	$Bi_{1.6}Pb_{0.4}$	$Bi_{1.7}Pb_{0.3}$		
	0.8	0.4	1.0	2.1	$Ru_{2.03(6)}O_{7.0(1)}$	$Ru_{0.85}O_{5.56}$	$Ru_{0.6}O_{4.42}$		
$BiPbRu_2O_{6.73}$	Bi	Pb	Ru	O					no
	10.4	8.1	18.6	62.7	$Bi_{1.14(6)}Pb_{0.89(7)}$	$Bi_{1.03}Pb_{0.97}$	$Bi_{1.36}Pb_{0.64}$		
	0.5	0.6	1.2	2.2	$Ru_{2.11)}O_{6.9(2)}$	$Ru_{0.75}O_{5.15}$	$Ru_{0.73}O_{5.44}$		
$Pb_2Ru_2O_{6.5}$	Pb	Ru	O						no
	18.5	20.3	61.3		$Pb_{2.0(1)}Ru_{2.2(2)}$	$Pb_2Ru_{1.14}$	$Pb_2Ru_{0.75}$		
	0.2	0.1	0.5		$O_{6.6(3)}$	$O_{9.5}$	$O_{6.59}$		

[a] The scraping is carried out on the pellet after impedance measurement with a flow of argon. For XPS results all the compositions are calculated considering the pyrochlore formula (Bi + Sr/Pb) = 2.

last point, one should keep in mind that the experimental results are strongly dependent on microstructural effects and quality of the deposited layer and of the electrode/electrolyte interface. For this reason, the comparison of ASR values from one study to another one should be manipulated carefully.

The fine analysis by SEM/XRD/XPS of the phase transformation at the electrode/electrolyte interface under working conditions is detailed below with evidence of the better stability for low bismuth substituted compounds.

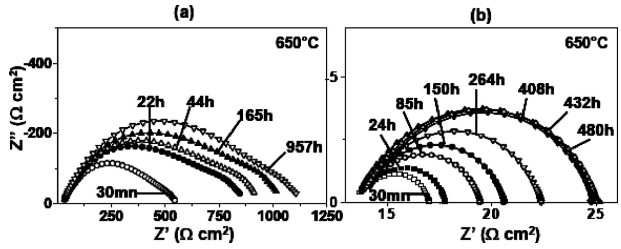

Figure 5. Evolution at 650 °C of Rp for (a) $Pb_2Ru_2O_{6.5}$ with no stabilization after 900 h and (b) $Bi_{1.9}Sr_{0.1}Ru_2O_{7-\delta}$ with stabilization after 400 h.

Table 3. Initial and Final Electrode Resistance Values ASR (Ω cm²) and Associated Stabilization Time (h) for Different $Bi_{2-x}Sr_xRu_2O_{7-\delta}$ and $Bi_{2-x}Pb_xRu_2O_{7-\delta}$ Solid Solutions

	x_{Sr} = 0	x_{Sr} = 0	x_{Sr} = 0.25	x_{Sr} = 0.5	x_{Pb} = 0.5	x_{Pb} = 1	x_{Pb} = 2
stabilization	yes	yes	yes	yes	yes	no	no
ASR (Ω cm²) initial value	3(1)	3(1)	4(1)	50(1)	7(1)	158(10)	493(10)
ASR (Ω cm²) final value	13(1)	12(1)	12(1)	98(2)	11(1)	319(10)	1085(10)
time (h)	300	450	350	50	400	>400	>400

4.4. Electrode Chemical Denaturation. Due to the limited electrochemical stability during electrochemical tests, a special attention has been paid to carefully analyze the deposited electrode before and after polarization through SEM, XRD, and XPS techniques.

At the microscopic scale, the SEM micrographs of the electrode surface and slice layer show no physical degradation after preliminary impedance measurements, and the adhesion between the electrolyte and the electrode appears preserved for all the tested compounds. This comparison is shown in Figure 4g,h,i for the parent $Bi_2Ru_2O_7$.

For the so-called "unstable" compositions, the XRD patterns of the electrode surfaces show a systematic appearance of more or less intense additional peaks (Figure 6). It has not been possible to establish a clear dependence of the intensities and 2θ positions function of the initial composition. Figure 6 shows three typical modifications after the electrochemical process. Surprisingly, $Bi_2Ru^{4+}{}_2O_7$, which is electrochemically stable, partially transforms into $Bi_3Ru^{4.33+}{}_3O_{11}$. By itself, this unedited result is a major obstacle of the possible use of the parent compound. However, the Rp stability while the compound progressively transforms remains rather obscure. It must be noted that both $Bi_2Ru_2O_7$ and $Bi_3Ru_3O_{11}$ have been tested as LT electrodes and both show attractive performances; however, this phase transformation was not detected [6,7] in this temperature range. For the other compositions, it has not been possible to identify the formed phases, but one should consider that both the working electrochemical conditions and the electrode/YSZ interface should favor the structural modification. At least, for the electrochemically "stable" compounds, XRD patterns are unchanged after impedance measurements, in good agreement with the correlation between the instability and the modification of the electrode. At least low substitution seems to favor the pyrochlore structural stabilization retraining attractive properties.

A compositional investigation of the observed denaturation was carried out by XPS analysis before and after impedance measurements. In any cases, initial powders show a strong

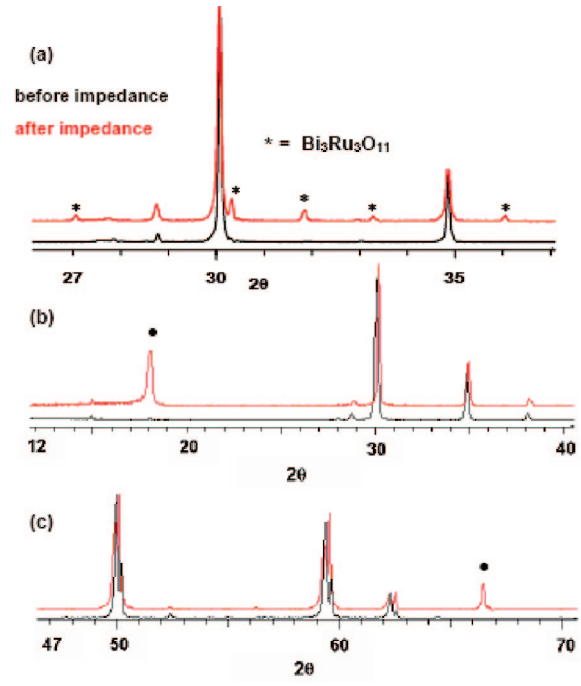

Figure 6. XRD patterns after impedance measurement of (a) $Bi_2Ru_2O_{7-\delta}$ and high substituted compounds (b) $BiPbRu_2O_{6.73}$ and (c) $Bi_{1.5}Sr_{0.5}Ru_2O_{7-\delta}$. (*) $Bi_3Ru_3O_{11}$ extra peaks, (●) not assigned.

surfacial deficit of ruthenium (Table 2). This should be related to the great volatility of ruthenium into the RuO_4 form at high temperature, possible at the synthesis stage, but one should keep in mind that the depth information is less than 100 Å. For $Bi_{1.75}Sr_{0.25}Ru_2O_{6.9}$, it has been checked that the composition reaches its expected value (Table 2) after a progressive etching of the surface with Ar^+.

For all the samples, a variation of composition at surface of the grains was observed previously and after the impedance measurements, consistent with an evolution of the structure under electrochemical reaction. However, in so-called "unstable" samples, the extra XRD peaks reported above are accompanied by a stronger evolution of the grain surface composition prior and after polarization. It is noteworthy that no general rule concerning the compositional changes has be established, for example, the Ru/M ratio increases for $x_{Sr} = 0.5$, remains unchanged for $x_{Pb} = 1$, and decreases for $x_{Pb} = 2$. However, the concept of a gradual alteration of the grain surface under electrochemical activity is put forward. For "unstable" samples, the whole grain is progressively damaged, yielding a continuous evolution of the resistance polarization. On the other hand, for low substitution, for example, "stable" compounds, as shown by the slight compositional variation before and after polarization, the grain degradation is limited, in good agreement with unchanged XRD patterns.

It is worth recalling that our measurements have been performed at temperatures greater than 600 °C due to the limited operating temperature of YSZ. The phase degradation should be reduced working at medium temperatures and using more adapted electrolytes like BiMEVOX or ESB.

4.5. Electrochemical Behavior. Here, we focused on the so-called "stable" compounds in order to fully investigate

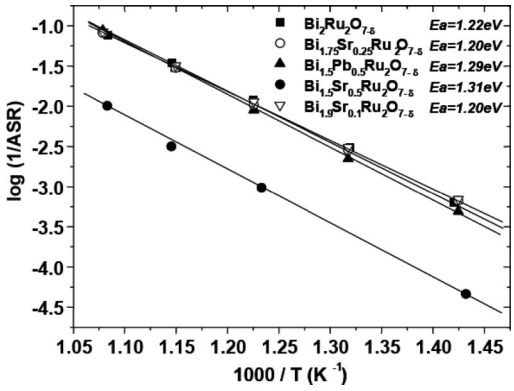

Figure 7. Arrhenius plots (1/ASR) and Ea of pertinent compounds.

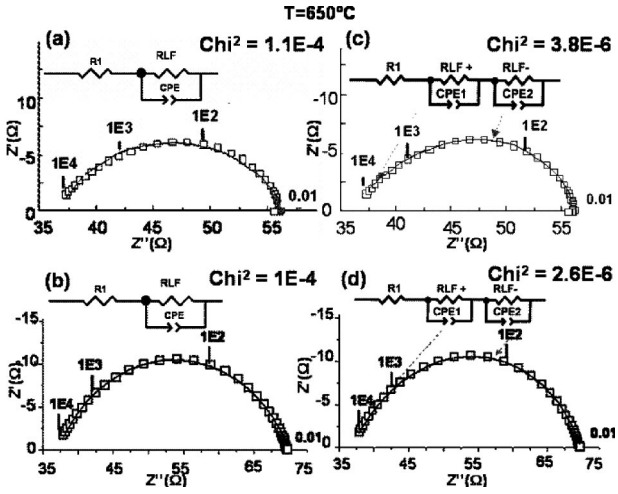

Figure 8. Equivalent circuit and corresponding fit to one contribution (RLF) for $Bi_{1.5}Pb_{0.5}Ru_2O_{7-\delta}$ (a) and $Bi_{1.9}Sr_{0.1}Ru_2O_{7-\delta}$ (b) and two contributions (RLF+, RLF−) (c, d), respectively, $T = 650$ °C.

the involved electrochemical mechanisms. Figure 7 shows the Arrhenius plot of the conductivity (1/ASR) and the associated activation energies (Ea) in air between 350 and 650 °C for $Bi_2Ru_2O_7$ and various substituted compounds. The Ea value and Arrhenius evolution of $Bi_2Ru_2O_7$ are comparable with those of the literature[6] and very close to those for $x_{Sr} = 0.1$, 0.25 and $x_{Pb} = 0.5$. On the other hand, the $x_{Sr} = 0.5$ substitution decreases the electrode performances.

In contradiction with the results of Mailley et al.,[6,7] which report for $Bi_2Ru_2O_7$ on 8YSZ, two temperature domains, with two different electrode reaction mechanisms associated (activation energy: Ea ~ 1.3 eV below 567 °C and ~ 1.0 eV above), we found only one activation energy in any case. However, Jaiswal et al.[10] have also observed a single process mechanism for $Bi_2Ru_2O_7$ on CGO with a value of Ea = 1.26 eV, close to our result (Ea = 1.22 eV), in the temperature range of 450−700 °C.

The cell impedance responses were fitted using an equivalent electric circuit for the three optimal compositions. In any case, the careful examination of the impedance diagrams shows a weak deformation at higher frequencies, but it is rather difficult to conclude to the contribution of one or two processes. First, a single contribution has been considered (resistance at low frequency: RLF); see Figure 8a,b at 650 °C for $x_{Pb} = 0.5$ and $x_{Sr} = 0.1$ (the corresponding

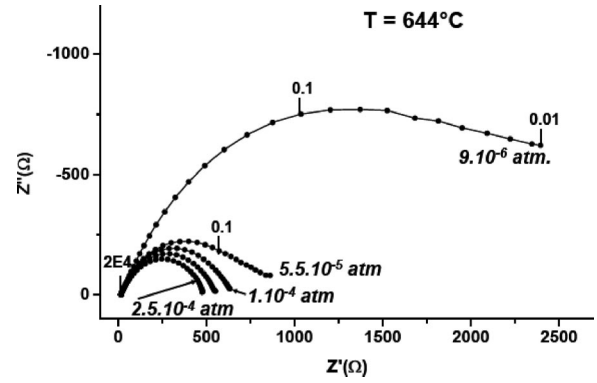

Figure 9. Impedance spectra of $Bi_{1.9}Sr_{0.1}Ru_2O_{7-\delta}$/YSZ/$Bi_{1.9}Sr_{0.1}Ru_2O_{7-\delta}$ cell on variable pO_2 for $T = 644$ °C.

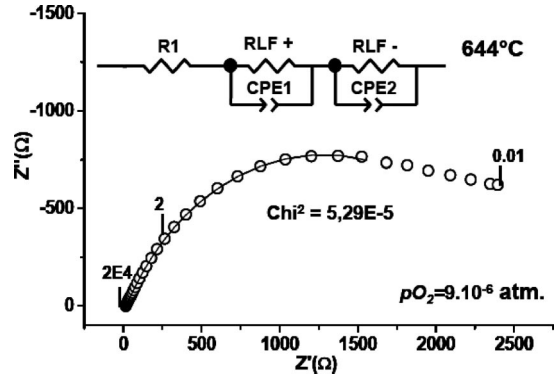

Figure 10. Equivalent circuit for two contributions e and corresponding fit (line) (RLF+, RLF−) for $Bi_{1.9}Sr_{0.1}Ru_2O_{7-\delta}$; $p_{O_2} = 9 \times 10^{-6}$ atm, $T = 644$ °C.

refined parameters are reported Table a in Supporting Information). In a second stage, it has been considered that the observed deformation at higher frequencies corresponds to an additional contribution RLF+ to be added to RLF−. The results of the fits are reported in Figure 11c,d (and table a in Supporting Information). An equivalent circuit using two contributions greatly increases the quality of the fit but remains doubtful due to the small number of points shaping the RLF+ shoulder. Then a unique RLF contribution model was preferred which matches the previous ASR estimated values.

On varying p_{O_2}, important changes are observed (Figure 9), resulting from the electrode sensitivity toward the oxygen through the reaction at the TPB: $^1/_2O_2 + e^- \leftrightarrows O^{2-}$.

All the studied compounds behave similarly. As an example, the impedance spectra under variable p_{O_2} is shown in Figure 9 for $Bi_{1.9}Sr_{0.1}Ru_2O_{7-\delta}$ at 650 °C. At low oxygen pressure, two different mechanisms prevail in the electrode reaction, fitted with two unambiguous contributions RLF+ and RLF− (Figure 10). When p_{O_2} decreases, the deformation RLF+ is accentuated but remains weak compared to RLF−. At low pressures ($p_{O_2} < 2 \times 10^{-4}$ atm) a third phenomenon is added at lower frequencies. However, the explored range of frequency is not sufficient for its investigation. Thus, we focused on RLF− and RLF+. The resistance versus p_{O_2} obeys the relation $ASR = (ASR)_0 \times (p_{O_2})^{-m}$,[10,38,39] m being

(38) Nagamoto, H.; Inoue, H. *J. Electrochem. Soc.* **1989**, *136*, 2088.
(39) Verkek, M. J.; Burggraaf, A. J. *J. Electrochem. Soc.* **1983**, *130*, 78.

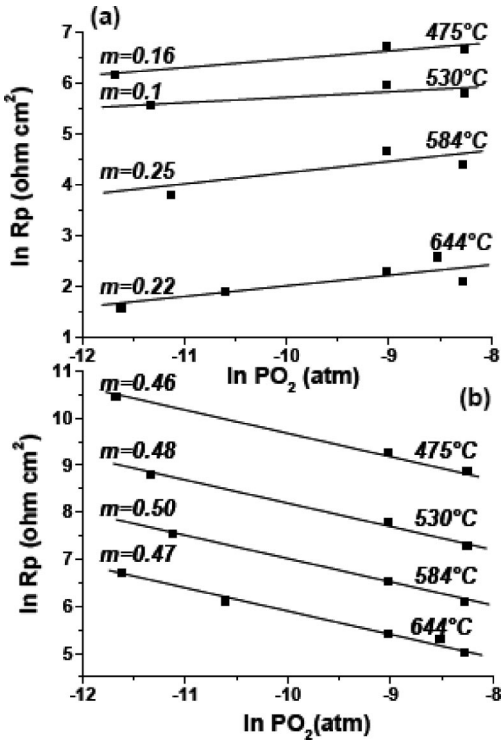

Figure 11. $Bi_{1.5}Pb_{0.5}Ru_2O_{7-\delta}$ ln(RLF+) (a) and ln(RLF−) (b) evolution within p_{O_2}.

the limiting step of the oxygen reduction reaction at the surface of the electrode. It follows that three main behaviors can be distinguished (i) $m = 1$, the diffusion of molecular oxygen in the electrode microstructure is the limiting factor, correlated to the porosity; (ii) $m = 0.5$, the limiting factor is the diffusion of the adsorbed oxygen from the electrode to the TBP; and (iii) $m = 0.25$, the limiting stage is the charge transfer at the TBP.

Figure 11a displays the evolution of RLF+ versus p_{O_2} for $Bi_{1.5}Pb_{0.5}Ru_2O_{7-\delta}$. The plotted m factor is ranging between 0.1 and 0.25, and then RLF+ is reminiscent of a limitation by the charge transfer at the TBP. Nevertheless, its slight evolution as a function of p_{O_2} stands within the error of the RLF+ value. Additional studies in a broader p_{O_2} range are necessary to validate these results.

The contribution associated with RLF− is much more sensitive to p_{O_2}, and the value of RLF− strongly increases on decreasing p_{O_2}. The m values vary from 0.46 to 0.5 (Figure 11b). This contribution is then correlated to the diffusion of the adsorbed species at the surface of the electrode. RLF− is predominant for all investigated p_{O_2} and temperatures. Then, the electrode activity is strongly influenced by the surface diffusion toward TBP. This observation has to be correlated with the metallic conducting character of these materials which limits the O^{2-} diffusion.

5. Conclusion

$Bi_{2-x}Pb_xRu_2O_{7-\delta}$ and $Bi_{2-x}Sr_xRu_2O_7$ solid solutions were studied with the aim to improve the catalytic properties of the Ru pyrochlore as well as their electric conductivity. As the parent $Bi_2Ru_2O_7$, all the studied materials remain metallic. However, for undoped compounds as well as for great x values, impedance spectroscopy revealed a strong time-dependent polarization resistance while deposited on YSZ. It is due to the formation of additional phases probably favored by the running conditions, never mentioned before. As an encouraging result, small x_{Sr} and x_{Pb} substitution stabilizes the phases while preserving their electrochemical properties. Keeping in mind the use of these stabilized pyrochlores for LT-SOFC, their reactivity with CGO has been tested which shows chemical reactivity between them. It justifies the use of YSZ during our study, but additional tests on bismuth based oxides (BiMEVOX or ESB) are currently under investigation. The electrode polarization process appears strongly limited by the surface diffusion toward the TBP, a result that one should correlate with their metallicity. However, their performances remain appreciable, and future efforts should be concentrated on the electrode layer porosity and grain-size control with respect to the so-called "stable" chemical compositions highlighted here.

Supporting Information Available: Figures of the resistivity evolution according to the temperature, in the 10 K to 1000 K range (a), and evolution of the characteristic magnetic susceptibility χ from ambient to 10K (b) (PDF).

Table of fits results of the impedance response at 650 °C, for $Bi_{1.9}Sr_{0.1}Ru_2O_{7-\delta}$, $Bi_{1.75}Sr_{0.25}Ru_2O_{6.9}$, and $Bi_{1.5}Pb_{0.5}Ru_2O_{7-\delta}$, with one and two equivalent circuit contributions, (PDF). This material is available free of charge via the Internet at http://pubs.acs.org.

CM801942C